IOP PUBLISHING NANOTECHNOLOGY
Nanotechnology **18** (2007) 424036 (6pp) doi:10.1088/0957-4484/18/42/424036

The effect of phonon scattering on the switching response of carbon nanotube field-effect transistors

M Pourfath and H Kosina

Institute for Microelectronics, TU Wien, Gußhausstraße 27–29/E360, 1040 Wien, Austria

E-mail: pourfath@iue.tuwien.ac.at

Received 2 April 2007, in final form 31 July 2007
Published 21 September 2007
Online at stacks.iop.org/Nano/18/424036

Abstract
The performance of carbon nanotube field-effect transistors is analyzed numerically, using the non-equilibrium Green's function formalism. The effect of electron–phonon scattering on both the DC and switching response of these devices is studied. For the calculation of the switching response, the quasi-static approximation is assumed. The role of the electron–phonon coupling strength and phonon energy are investigated. Our results indicate that scattering with high-energy phonons reduces the on-current only weakly, but can increase the switching time considerably due to charge pile-up in the channel. Conversely, scattering with low-energy phonons reduces the on-current more effectively, but has a weaker effect on the switching time.

(Some figures in this article are in colour only in the electronic version)

1. Introduction

Tremendous advances have been achieved in microelectronics technology during the past decades. With continuing efforts to improve the speed and functionality of integrated circuits and to achieve higher integration densities, device dimensions are being decreased, and they will eventually reach the scale of the electron wavelength. With the aid of numerical analysis one can gain a deeper insight into device operation and investigate methods to improve the device performance. Carbon nanotube field-effect transistors (FETs) have been considered in recent years as potential alternatives to complementary metal–oxide–silicon (CMOS) devices.

A carbon nanotube (CNT) can be viewed as a rolled-up sheet of graphene with a diameter of a few nanometers. The way the graphene sheet is wrapped is represented by a pair of indices (n, m), called the chiral vector. The integers n and m denote the number of basis vectors along two directions in the honeycomb crystal lattice of graphene. The CNT is called *zigzag*, if $m = 0$, *armchair*, if $n = m$, and *chiral* otherwise. CNTs with $n - m = 3$ are metals, otherwise they are semiconductors [1]. Semiconducting CNTs can be used as channels for transistors [2] which have been studied in recent years as potential alternatives to CMOS devices because of their capability of quasi-ballistic transport.

Depending on the work function difference between the metal contact and the CNT, carriers at the metal–CNT interface encounter different barrier heights (see figure 1). The fabrication of devices with positive (Schottky-type) [3] and zero (ohmic) [4] barrier heights for holes has been reported. In this work we consider devices with zero barrier heights for electrons.

The non-equilibrium Green's function (NEGF) method has been successfully utilized to investigate the characteristics of nanoscale silicon transistors [5], carbon nanotube (CNT)-based transistors [6], and molecular devices [7, 8]. In this work we employ the NEGF formalism to study quantum transport in CNT-based transistors in more detail.

2. The non-equilibrium Green's function formalism

The NEGF formalism initiated by Schwinger, Kadanoff and Baym allows one to study the time evolution of a many-particle quantum system. Knowing the single-particle Green's functions of a given system, one may evaluate single-particle quantities such as carrier density and current. The many-particle information about the system is cast into self-energies, which are part of the equations of motion for the Green's functions. Perturbation expansion of the Green's functions is the key to approximating the self-energies. Green's functions

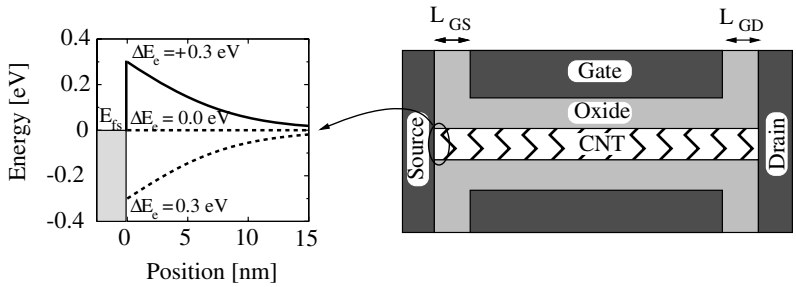

Figure 1. Sketch of the CNT-FET investigated. The insulating layer is HfO_2 with $\epsilon_r = 15$ and a thickness of 2 nm. The geometry parameters are $L_{GS} = L_{GD} = 4$ nm and $L_{CNT} = 50$ nm. ΔE_c represents the Schottky barrier at the metal–CNT interface.

provide a powerful technique to evaluate the properties of a many-body system both in thermodynamic equilibrium and non-equilibrium situations.

Four types of Green's functions are defined: the retarded and advanced Green's functions, G^r and G^a, which deal with the dynamics of carriers, and lesser and greater Green's functions, $G^<$ and $G^>$, which describe the statistics. The transport equations are solved on the surface of the CNT. Due to quantum confinement along the tube circumference, wavefunction of carriers are bound around the CNT and can propagate along the tube axis. We considered an azimuthal symmetric structure, in which the gate fully surrounds the CNT. Under the assumption that the potential profile does not vary sharply along the CNT, the sub-bands are decoupled [9]. As a result, the transport equations need to be solved only along the CNT axis, which is assumed to be the z-direction in cylindrical coordinates. In this work we assume bias conditions for which the first sub-band contributes mostly to the total current. In the mode-space approach the transport equation for a sub-band can be written as [6, 10]

$$G^{r,a}(z,z';E) = [EI - H(z,z';E) - \Sigma^{r,a}(z,z';E)]^{-1}, \quad (1)$$

$$G^{\lessgtr}(z,z';E) = G^r(z,z';E)\Sigma^{\lessgtr}(z,z';E)G^a(z,z';E), \quad (2)$$

where the self-energy Σ describes the renormalization of the Green's function due to the interaction with the surrounding many-particle system, and H is the single-particle Hamiltonian. The general form of the single-particle Hamiltonian is given by

$$H(z) = -\frac{\hbar^2}{2m}\nabla_z + U(z), \quad (3)$$

where the potential energy U includes the effects of the lattice potential and the Hartree potential, which is in fact the solution of the Poisson equation.

In order to solve the system of equations discussed above in a finite system, boundary conditions have to be specified. The boundary conditions of equation (1) have to model the contacts, which act as a source or drain for electrons. Due to the transitions between the device and the lead, this type of boundary condition can be imposed by adding self-energies [5, 11, 10]. The self-energies due to contacts are only non-zero at the boundaries [10] and can be calculated as in [10, 12, 6].

Using a perturbation expansion, one can define the self-energy Σ as an irreducible part of the Green's function. An exact evaluation of the self-energy is possible only for some rather pathological models. For real systems one has to rely on approximation schemes. In this work, the lowest-order self-energy for electron–phonon interaction within the self-consistent Born approximation has been applied [10].

The interaction of electrons with optical phonons is inelastic. Assuming that the electron–phonon interaction occurs locally [13], $\Sigma(\mathbf{r},\mathbf{r}';E) = 0$ for $\mathbf{r} \neq \mathbf{r}'$, the self-energies can be written as

$$\Sigma^<_{inel}(E) = \sum_j D_{inel,\lambda}\left(n_B(\hbar\omega_\lambda) + \tfrac{1}{2} \pm \tfrac{1}{2}\right) G^<(E \pm \hbar\omega_\lambda),$$

$$\Sigma^>_{inel}(E) = \sum_j D_{inel,\lambda}\left(n_B(\hbar\omega_\lambda) + \tfrac{1}{2} \pm \tfrac{1}{2}\right) G^>(E \mp \hbar\omega_\lambda), \quad (4)$$

where $\hbar\omega_\lambda$ denotes the phonon energy of branch λ, $n(\hbar\omega_\lambda)$ the average phonon occupation number, and D_λ the electron–phonon coupling strength. The plus and minus signs in equation (4) denote the phonon emission and absorption processes, respectively. Assuming that the bath of phonons is maintained in thermodynamic equilibrium, $n(\hbar\omega_\lambda)$ is given by the Bose–Einstein distribution function. The electron–phonon interaction strength of an $(n, 0)$ zigzag CNT is given by

$$D_{inel} = \frac{\hbar|M^{OP}_\lambda|^2}{2nm_c\omega_\lambda}, \quad (5)$$

where m_c is the mass of a carbon atom. Interaction with acoustic phonons can be approximated as an elastic process, $E \pm \hbar\omega_\lambda \approx E$, and the approximation $n_B(\hbar\omega_\lambda) \approx n_B(\hbar\omega_\lambda) + 1 \approx k_BT/\hbar\upsilon_\lambda q$, where υ is the sound velocity, can be used. Based on this approximation, the self-energies for acoustic phonon interaction simplify to

$$\Sigma^{\lessgtr}_{el}(E) = D_{el}G^{\lessgtr}(E), \quad (6)$$

$$D_{el} = \frac{k_BT|M^{AP}_\lambda|^2}{nm_c\upsilon_\lambda}. \quad (7)$$

Phonons with $\mathbf{q} \approx 0$ are referred to as Γ-point phonons, and can belong to the twisting acoustic (TW), the longitudinal acoustic (LA), the radial breathing mode (RBM), the out-of-phase out-of-plane optical branch (ZO), the transverse optical (TO), or the longitudinal optical (LO) phonon branch. Phonons inducing inter-valley transitions have a wavevector of $|\mathbf{q}| \approx q_K$, where q_K corresponds to the wavevector of the K-point of the Brillouin zone of graphene. K-point phonons, also referred

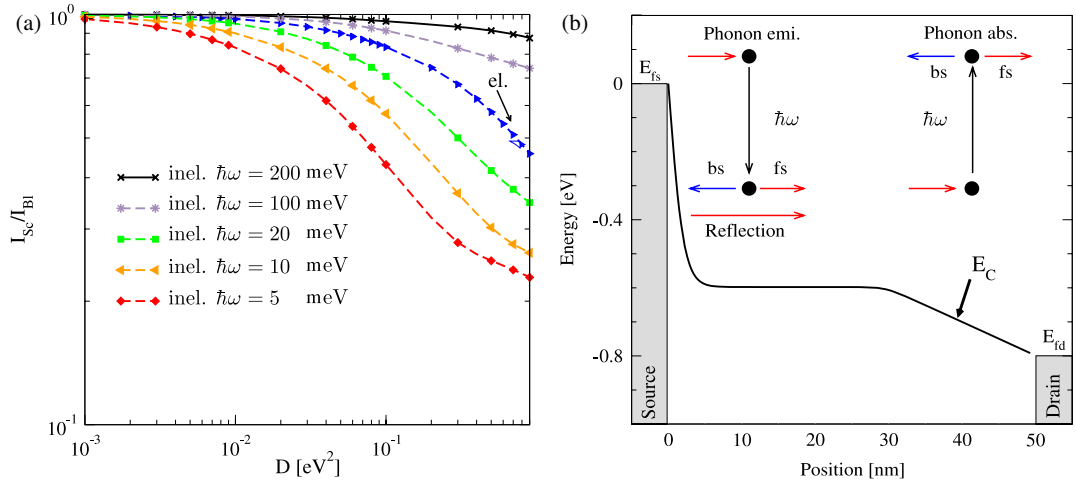

Figure 2. (a) Ballisticity versus electron–phonon coupling strength for a CNT of 50 nm length. Results for both elastic and inelastic scattering with different phonon energies are shown. The operating point is $V_G = V_D = 1$ V. The dependence of the ballisticity as a function of the bias is discussed in [19]. (b) Sketch of phonon emission and absorption processes in the channel. E_c is the conduction band of the CNT.

to as zone boundary phonons, are a mixture of fundamental polarizations.

The self-energy due to electron–phonon interaction comprises the contributions of elastic and inelastic scattering mechanisms, $\Sigma_{e-ph} = \Sigma_{el} + \Sigma_{inel}$. The retarded self-energy is given by

$$\Sigma^{r}_{e-ph}(E) = -\frac{i}{2}\Gamma_{e-ph}(E) + P\int \frac{dE'}{2\pi}\frac{\Gamma_{e-ph}(E')}{E-E'}, \quad (8)$$

where $\Gamma_{e-ph} \equiv i(\Sigma^{>}_{e-ph} - \Sigma^{<}_{e-ph})$ defines the broadening, and $P\int$ represents the principal part of the integration. The imaginary part of the retarded self-energy broadens the density of states, whereas the real part shifts it in energy.

3. Implementation

The coupled system of transport and Poisson equations was solved numerically. In order to solve transport equations numerically, they need to be discretized in both the spatial and the energy domain. Uniform spatial grids have been employed. The carrier concentration at some node l and the current density between the nodes l and $l+1$ of the device are given by

$$n_l = -4i\int \frac{dE}{2\pi} G^{<}_{l,l}(E), \quad (9)$$

$$j_{l,l+1} = \frac{4q}{\hbar}\int \frac{dE}{2\pi} 2\Re e\{G^{<}_{l,l+1}(E)t_{l+1,l}\}, \quad (10)$$

where the factor 4 is due to the spin and band degeneracy. In the Poisson equation carriers are treated as a sheet charge distributed over the surface of the CNT [14, 15]. The energy grid, however, should be non-uniform, since an adaptive integration method is generally required to evaluate quantities such as (9) with sufficient accuracy.

The coupled system of the transport and Poisson equations has to be solved self-consistently [8], where the convergence of the self-consistent iteration is a critical issue. To achieve convergence, fine resonances at some energies in (9) have to be resolved accurately [15, 16]. For that purpose an adaptive method for selecting the energy grid is essential [16].

4. The effect of electron–phonon interaction

The electron–phonon coupling strength and the phonon energy depend on the chirality and the diameter of the CNT [17, 18]. In this section the device response is studied for a wide range of electron–phonon interaction parameters. All the simulations were performed for the device shown in figure 1.

4.1. Electron–phonon coupling strength

Figure 2(a) shows the ballisticity as a function of the electron–phonon coupling strength. The ballisticity is defined as I_{Sc}/I_{Bl}, the ratio of the on-current in the presence of electron–phonon interaction to the current in the ballistic case [19].

The left-hand part of figure 2(b) illustrates an electron losing its kinetic energy by emitting a phonon. The electron will be scattered either forward or backward. In the case of backward scattering the electron faces a thick barrier near the source contact and will be reflected with high probability, such that its momentum will again be directed towards the drain contact.

Elastic scattering conserves the energy of carriers, but the current decreases due to the elastic back-scattering of carriers. Figure 3 shows the spectrum of the current density at the source and drain contact. For elastic scattering, the source and drain current spectra are symmetric (see figure 3). As the electron–phonon coupling strength increases, resonances in the current spectrum disappear, and the total current decreases due to elastic back-scattering. In the case of inelastic scattering, carriers acquiring enough kinetic energy can emit a phonon and scatter into lower-energy states. Therefore, as shown in figure 3(b), the source and drain current spectra are not symmetric.

4.2. Phonon energy

Figure 4(a) shows the dependence of the ballisticity with respect to the phonon energy. With increasing phonon energy the effect of phonon scattering on the current is

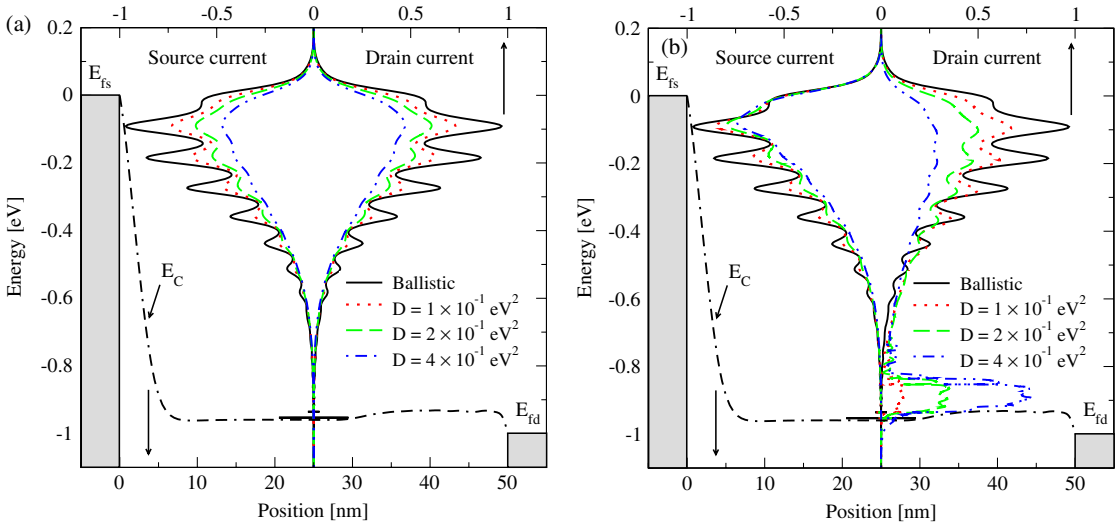

Figure 3. The spectra of the source and drain currents. (a) The effect of elastic phonon scattering with different coupling strengths is shown. As the coupling strength increases resonances in the current spectrum disappear, and the total current decreases due to elastic back-scattering. (b) The effect of inelastic phonon scattering with different coupling strengths is shown. The phonon energy is $\hbar\omega = 100$ meV. Carriers acquiring enough kinetic energy can emit phonons and scatter into lower-energy states. Since the energy of the electrons is not conserved in this process, the source and drain current spectrum are not symmetric. As the coupling strength increases, more electrons are scattered into lower-energy states.

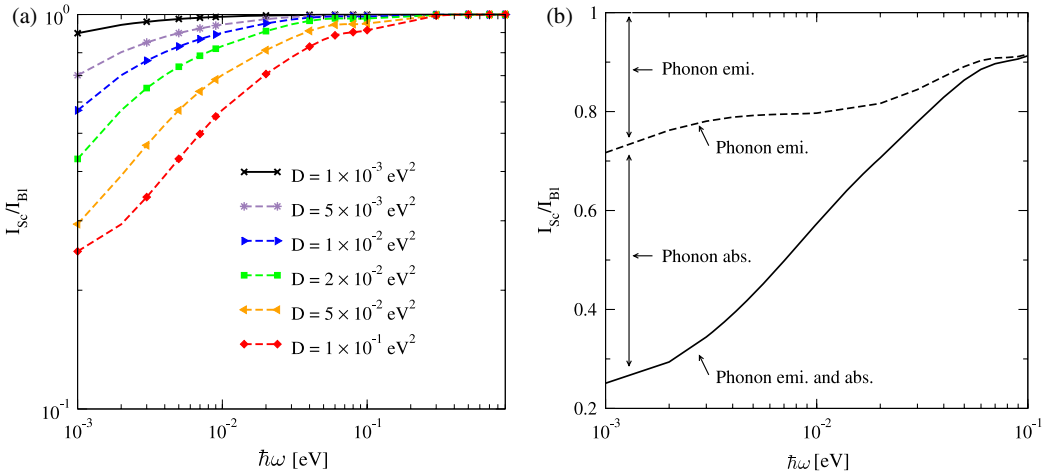

Figure 4. (a) Ballisticity versus phonon energy for a CNT of 50 nm length. Results for inelastic scattering with different electron–phonon couplings are shown. $V_G = V_D = 1$ V. (b) Ballisticity versus phonon energy with $D = 10^{-1}$ eV^2 at the bias point $V_G = V_D = 1$ V. The contributions due to phonon absorption and emission are shown.

reduced, because scattered electrons lose more kinetic energy and the probability for traveling back to the source contact decreases. The considerable decrease of ballisticity for low-energy phonons is due to the phonon absorption process.

The right-hand part of figure 2(b) shows an electron absorbing energy from a phonon and scattering into a higher-energy state. In this case, the probability for arriving at the source contact increases. This process can severely reduce the total current [19].

Figure 4(b) separately shows the effects of the phonon emission and absorption processes on the ballisticity. As the phonon energy decreases, the phonon occupation number increases exponentially, and the self-energy contributions of these two components increase. However, due to the higher probability for back-scattering of electrons in the case of phonon absorption, this component reduces the total current more effectively than the phonon emission process does.

To illustrate the effect of electron–phonon interaction on the switching response of the device, the gate-delay time τ is studied:

$$\tau = \frac{C_G V_G}{I_D}. \tag{11}$$

Here, ${C_G}^{-1} = {C_{Ins}}^{-1} + {C_Q}^{-1}$. The quantum capacitance can be approximated as $C_Q \approx 8q^2/h\nu_F \approx 400\text{aF}/\mu\text{m}$, including the twofold band and spin degeneracy [20, 15]. Assuming the quantum capacitance limit [21] ($C_Q \ll C_{Ins}$), one gets $C_G \approx C_Q$ and, therefore, $C_G V_G \approx Q_{Ch}$, where Q_{Ch} is the

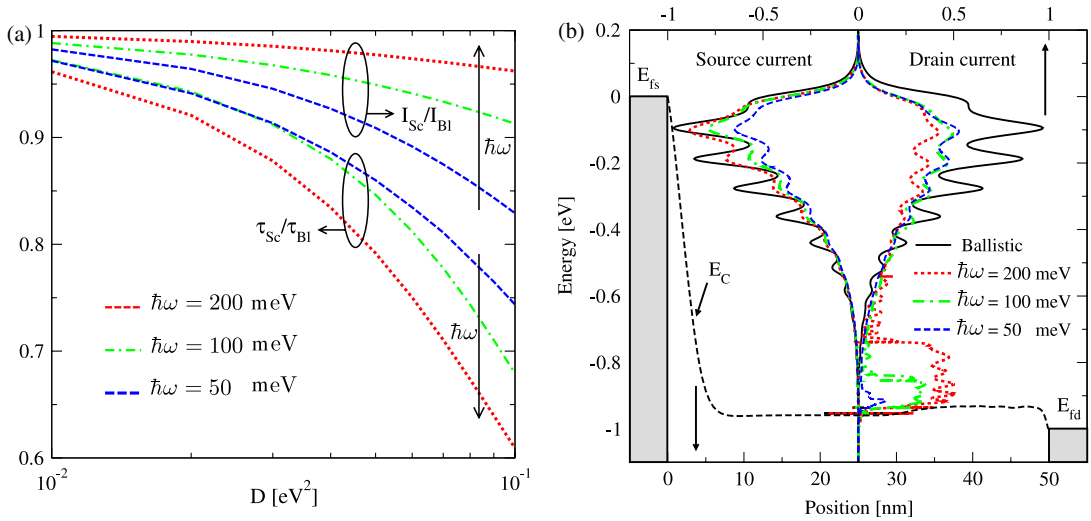

Figure 5. (a) The ratio of the gate-delay time in the presence of electron–phonon interaction to the gate-delay time in the ballistic case, τ_{Sc}/τ_{Bl}, as a function of the electron–phonon coupling strength. For comparison, the ratio I_{Sc}/I_{Bl} is also shown. As the phonon energy increases, the gate-delay time increases. This behavior is due to the reduction of the electron velocity in the channel and the resulting charge pile-up. (b) The spectra of the source and drain currents. The effect of inelastic scattering with different phonon energies is shown. The electron–phonon coupling strength is $D = 2 \times 10^{-1}$ eV^2. The figure shows a considerable increase of the electron population close to the conduction band-edge as the phonon energy increases.

total charge in the CNT channel. As a result,

$$\tau \approx \frac{Q_{Ch}}{I_D}. \tag{12}$$

It has been shown that, for CNT-based transistors, the quasi-static approximation assumed here is justified for frequencies below THz [22].

Figure 5(a) shows the ratio of the gate-delay time in the presence of electron–phonon interaction to that in the ballistic case, τ_{Sc}/τ_{Bl}, as a function of the electron–phonon coupling strength. As the phonon energy increases, the gate-delay time increases. This behavior can be attributed to the average electron velocity in the channel, which is high for ballistic electrons and low for electrons scattered to lower-energy states.

Figure 5(b) shows the spectra of the source and drain currents for different inelastic phonon energies. Electrons can emit a single phonon or a couple of phonons to reach lower-energy states. The probability of multiple phonon emissions decreases as the number of interactions increases. Therefore, as the phonon energy increases, the occupation of electrons at lower-energy states increases.

As shown in figure 5(b), the electron population close to the conduction band-edge considerably increases as the phonon energy increases. Therefore, as the phonon energy increases, the mean velocity of electrons decreases and the carrier concentration in the channel increases (figure 6). The increased charge in the channel results in an increased gate-delay time.

4.3. Discussion

CNTs with a diameter $d_{CNT} > 2$ nm have a band gap $E_G < 0.4$ eV, which render them unsuitable as a channel for transistors. Since the fabrication of devices with a diameter $d_{CNT} < 1$ nm is very difficult, we limit our study to zigzag CNTs with diameters in the range of $d_{CNT} = 1$–2 nm.

Scattering with acoustic phonons is treated as an elastic process. The electron–phonon coupling is also weak for acoustic phonons ($D_{AP} < 10^{-3}$ eV^2), which implies that the elastic back-scattering of carriers is weak. Inelastic scattering is induced by OP, RBM, and K-point phonons. Considering the class of CNTs discussed above, the energies of the these phonons are $\hbar\omega_{OP} \approx 200$ meV, $\hbar\omega_{RBM} \approx 25$ meV, and $\hbar\omega_{K_1} \approx 160$ meV and $\hbar\omega_{K_2} \approx 180$ meV [23, 19]. The corresponding coupling coefficients are $D_{OP} \approx 40 \times 10^{-3}$ eV^2, $D_{RBM} \approx 10^{-3}$ eV^2, and $D_{K_1} \approx 10^{-4}$ eV^2, and $D_{K_2} \approx 10^{-3}$ eV^2 [19].

As discussed in section 4.2, high-energy phonons such as OP and K-point phonons reduce the on-current only weakly, but can increase the gate-delay time considerably due to charge pile-up in the channel. Low-energy phonons such as the RBM phonon can reduce the on-current more effectively, but have a weaker effect on the gate-delay time. In a CNT at room temperature, the scattering processes are mostly due to electron–phonon interaction with high-energy phonons. Therefore, the on-current of short CNT-FETs can be close to the ballistic limit [4, 24, 25], whereas the gate-delay time can be significantly below that limit [26–28]. The intrinsic (without parasitic capacitances) gate-delay time for the ballistic case can be approximated as $\tau \approx 1.7$ ps μm^{-1}, or equivalently $f_T \approx 100$ GHz μm^{-1} [29]. The highest reported intrinsic cut-off frequency for a device with a length of 300 nm is $f_T \approx 30$ GHz [30], which is far below the ballistic limit. Inelastic electron–phonon interaction with high-energy phonons has to be considered to explain the results.

5. Conclusions

The effect of the electron–phonon interaction parameters on the performance of CNT-based transistors was studied numerically, using the NEGF formalism. We showed that

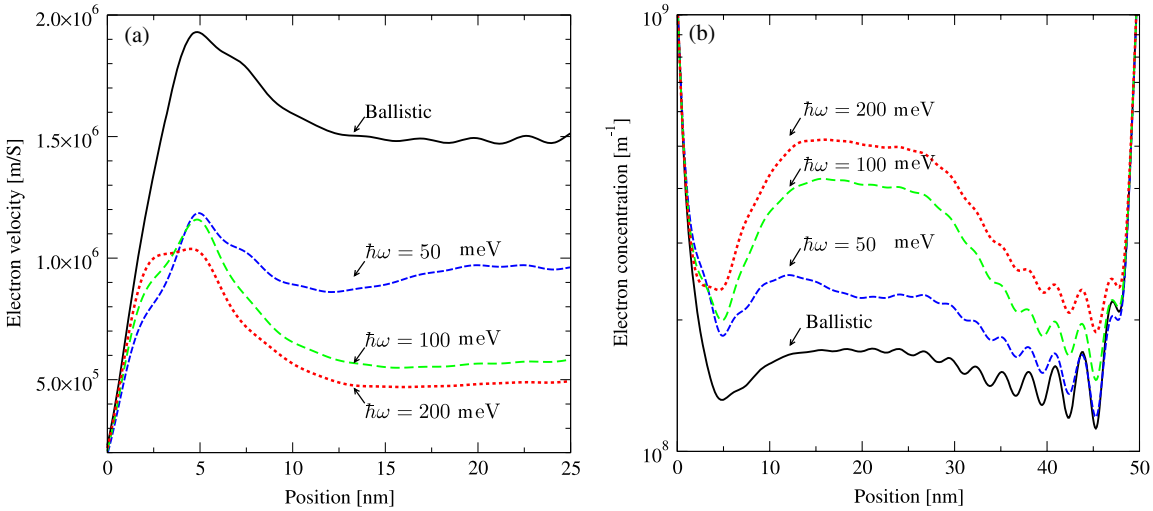

Figure 6. (a) The profile of the electron velocity near the source contact. (b) The profile of the electron concentration along the device. The results for the ballistic case and for electron–phonon interaction are shown. As the phonon energy increases, the electrons scatter to lower-energy states. Therefore, the electron velocity decreases and the carrier concentration increases. The electron–phonon coupling strength is $D = 10^{-1}$ eV^2 and the bias point is $V_G = V_D = 1$ V.

elastic back-scattering reduces the on-current effectively, but the strength of this process is weak in CNTs. Inelastic scattering with high-energy phonons reduces the on-current only weakly, but increases the switching time considerably, due to charge pile-up in the channel. Scattering with low-energy phonons reduces the on-current more effectively, but has a weaker effect on the switching time. In a CNT at room temperature, the scattering processes are mostly due to electron–phonon interaction with high-energy phonons. Therefore, the on-current of CNT-FETs can be close to the ballistic limit, whereas the switching time is found to be significantly below that limit.

Acknowledgments

This work, as part of the European Science Foundation EUROCORES Programme FoNE, was supported by funds from FWF, CNR, EPSRC and the EC Sixth Framework Programme, under Contract No. ERAS-CT-2003-980409.

References

[1] Saito R, Dresselhaus G and Dresselhaus M 1998 *Physical Properties of Carbon Nanotubes* (London: Imperial College Press)
[2] Martel R, Schmidt T, Shea H, Hertel T and Avouris P 1998 *Appl. Phys. Lett.* **73** 2447–9
[3] Appenzeller J, Radosavljevic M, Knoch J and Avouris P 2004 *Phys. Rev. Lett.* **92** 048301
[4] Javey A, Guo J, Wang Q, Lundstrom M and Dai H 2003 *Nature* **424** 654–7
[5] Svizhenko A, Anantram M P, Govindan T R, Biegel B and Venugopal R 2002 *J. Appl. Phys.* **91** 2343–54
[6] Svizhenko A and Anantram M 2005 *Phys. Rev.* B **72** 085430
[7] Tian W, Datta S, Hong S, Reifenberger R, Henderson J I and Kubiak C P 1998 *J. Chem. Phys* **109** 2874–82
[8] Ghosh A W, Rakshit T and Datta S 2004 *Nano Lett.* **4** 565–8
[9] Venugopal R, Ren Z, Datta S, Lundstrom M and Jovanovic D 2002 *J. Appl. Phys.* **92** 3730–9
[10] Datta S 1995 *Electronic Transport in Mesoscopic Systems* (New York: Cambridge University Press)
[11] Lake R, Klimeck G, Bowen R C and Jovanovic D 1997 *J. Appl. Phys.* **81** 7845–69
[12] Guo J, Datta S, Lundstrom M and Anantram M 2004 *The Int. J. Multiscale Comput. Eng.* **2** 257–78
[13] Lake R and Datta S 1992 *Phys. Rev.* B **45** 6670–85
[14] Pourfath M, Ungersboeck E, Gehring A, Park W J, Cheong B H, Kosina H and Selberherr S 2005 *Microelectron. Eng.* **81** 428–33
[15] John D, Castro L, Pereira P and Pulfrey D 2004 *Proc. NSTI Nanotech* vol 3, pp 65–8
[16] Pourfath M and Kosina H 2006 *Large-Scale Scientific Computing* (*Lecture Notes Comput. Sci.*) vol 3743 (Springer) pp 34–6
[17] Mahan G D 2003 *Phys. Rev.* B **68** 125409
[18] Popov V N and Lambin P 2006 *Phys. Rev.* B **74** 075415
[19] Koswatta S O, Hasan S, Lundstrom M, Anantram M P and Nikonov D E 2006 *Appl. Phys. Lett.* **89** 023125
[20] Burke P 2004 *Solid-State Electron.* **48** 1981–6
[21] John D, Castro L and Pulfrey D 2004 *J. Appl. Phys.* **96** 5180–4
[22] Chen Y, Ouyang Y, Guo J and Wu T X 2006 *Appl. Phys. Lett.* **89** 203122
[23] Park J, Rosenblatt S, Yaish Y, Sazonova V, Ustunel H, Braig S, Arias T, Brouwer P and McEuen P 2004 *Nano Lett.* **4** 517–20
[24] Guo J, Javey A, Dai H and Lundstrom M 2004 *IEDM Tech. Dig.* (San Francisco, CA: IEEE) pp 703–6
[25] Javey A, Guo J, Farmer D, Wang Q, Yenilmez E, Gordon R, Lundstrom M and Dai H 2004 *Nano Lett.* **4** 1319–22
[26] Singh D, Jenkins K, Appenzeller J, Neumayer D, Grill A and Wong H S P 2004 *IEEE Trans. Nanotechnol.* **3** 383–7
[27] Frank D and Appenzeller J 2004 *IEEE Electron Devices Lett.* **25** 34–6
[28] Huo X, Zhang M, Chan P C H, Liang Q and Tang Z K 2004 *IEDM Tech. Dig.* (San Francisco, CA: IEEE) pp 691–4
[29] Yoon Y, Ouyang Y and Guo J 2006 *IEEE Trans. Electron Devices* **53** 2467–70
[30] Louarn A L, Kapche F, Bethoux J M, Happy H, Dambrine G, Derycke V, Chenevier P, Izard N, Goffman M F and Bourgoin J 2007 *Appl. Phys. Lett.* **90** 233108